

# Brain tumor MRI Classification using a Novel Deep Residual and Regional CNN

Mirza Mumtaz Zahoor <sup>1,2</sup>, Saddam Hussain Khan <sup>3\*</sup>

1 Department of Computer & Information Sciences(DCIS), Pakistan Institute of Engineering and Applied Sciences (PIEAS), Islamabad 45650, Pakistan; [mumtazzahoor5@gmail.com](mailto:mumtazzahoor5@gmail.com) (M.M.Z.);

2 Faculty of Computer Sciences, Ibadat International University, Islamabad, Pakistan

3 Department of Computer Systems Engineering, University of Engineering and Applied Science (UEAS), Swat, Pakistan; [saddamhkhan@ueas.edu.pk](mailto:saddamhkhan@ueas.edu.pk) (S.H.K.)

Corresponding author: (e-mail: [saddamhkhan@ueas.edu.pk](mailto:saddamhkhan@ueas.edu.pk)).

## Abstract:

Brain tumor classification is crucial for clinical analysis and an effective treatment plan to cure patients. Deep learning models help radiologists to accurately and efficiently analyze tumors without manual intervention. However, brain tumor analysis is challenging because of its complex structure, texture, size, location, and appearance. Therefore, a novel deep residual and regional-based Res-BRNet Convolutional Neural Network (CNN) is developed for effective brain tumor (Magnetic Resonance Imaging) MRI classification. The developed Res-BRNet employed Regional and boundary-based operations in a systematic order within the modified spatial and residual blocks. Moreover, the spatial block extract homogeneity and boundary-defined features at the abstract level. Furthermore, the residual blocks employed at the target level significantly learn local and global texture variations of different classes of brain tumors. The efficiency of the developed Res-BRNet is evaluated on a standard dataset; collected from Kaggle and Figshare containing various tumor categories, including meningioma, glioma, pituitary, and healthy images. Experiments prove that the developed Res-BRNet outperforms the standard CNN models and attained excellent performances (accuracy: 98.22%, sensitivity: 0.9811, F-score: 0.9841, and precision: 0.9822) on challenging datasets. Additionally, the performance of the proposed Res-BRNet indicates a strong potential for medical image-based disease analyses.

**Keywords:** Brain ; Tumors; Classification; Deep Learning; Convolutional Neural network; MRI

---

## 1. INTRODUCTION

The human brain is among the body's most complicated and imperative organs, governing the neurological system. The most deadly brain tumor is caused by erratic and out-of-control cell growth in the brain [1]. Patient Survival depends on the type of glioma type; lowgrade gliomas have survival rates of 5 years as high as 80%, whereas survival rates of 5 years are under 5% for high-grade gliomas [2]. Timely brain tumor recognition and categorization is an imperative research topic in the clinical imaging domain, and it assists in choosing the most suitable treatment plan for a patient's life-saving [3].

Several screening methods, either invasive or non-invasive, are employed to identify tumors in the human brain [4]. Magnetic resonance imaging (MRI) is a preferable less harmful scanning modality since it provides rich information about the location of brain tumors, shape, and size in medical images (MI) and is generally considered quicker, cheaper, and safer [5]. Manual assessment of brain MR scans is challenging for radiologists to identify and categorize brain tumors from MIs. A computer-aided diagnosis (CADx) is required to reduce the burden as well as to assist radiologists or doctors with MI assessment.

Many research areas are being explored in medical image analysis. It included medical imaging domains like identification, detection, and segmentation [6]–[11]. Traditional ML approaches comprise numerous steps, pre-processing, feature extraction and selection, and classification. More discriminative feature acquisition is essential, as classification accuracy relies on obtained features.

In conclusion, the conventional ML techniques have two key challenges in the feature extraction step. One, it solely emphasizes low- or high-level attributes. Secondly, standard ML techniques rely on hand-crafted features that require significant prior knowledge, such as the position of the tumour in a medical scan, although there is a considerable risk of human error. Designing an effective system to incorporate high- and low-level features with no human intervention is crucial. As brain tumor datasets are being expanded, there is a need for technological improvements in feature extraction focusing on confined and imbalanced MR imaging data sets of brain abnormalities and other irregularities of the human organs[12] [13].

Recently, deep learning (DL) methods have frequently been employed for brain MRI categorization [14] While feature mining and classification were integrated into self-learning, deep learning methods do not necessitate a manual process for feature extraction. The DL approach requires a dataset, and minimal pre-processing is required for selecting salient features in a self-learning way [15]. MR imaging categorization faces a major challenge in diminishing the semantic space among high-level spatial details observed by a

---

human assessor and low-level acquired using the imagery mechanism. One of the well-known neural network models, convolutional neural networks (CNNs), specially designed for images, is utilized for feature extraction to acquire the important characteristics to categorize and minimize the semantic gap.

Recently, in many studies, CNNs are employed to classify brain MRI, and validate them on a dataset of brain tumors [16]–[20]. A deep CNN-based model was proposed in [21] for brain MRI images categorization into distinct classes. The authors employed brain MRI images from a publicly available dataset to prevent model ambiguity. The suggested model has a classification accuracy of 91.4%. Deepak and Ameer [22] employed a pre-train deep CNN, GoogLeNet, to extract key attributes using brain MR images and classify tumors into three classes with 98% accuracy. Ahmet and Muhammad [23] categorized brain MR images using various CNN models and attained satisfactory accuracy. They modify a pre-trained ResNet-50 DCNN by excluding the final five layers and introducing additional eight layers. Model achieved the highest among all pre-trained models accuracy of 97.2 %. Sultan et al. [24] suggested a CNN-based deep learning model utilizing two publicly accessible datasets have 3064 (glioma, meningioma, and pituitary tumors) and 516 (Grade II, Grade III, and Grade IV) brain medical scans. The proposed method has the best accuracy of 96.13 % and 98.7 %. Khwaldeh et al. [25] used several CNNs to classify brain MRI images and achieved good results. Using modified pre-trained Alexnet CNN, they achieved a higher accuracy of 97.2 %. Khan, M.A. et al. [26] developed a multi-model-based technique to differentiate brain tumors with DL. The presented system includes many stages. They used partial least squares (PLS) to concatenate the features and, ELM for classification. Their methodology stated improvement of 97.8%, 96.9%, and 92.5% on BraTs-2015, BraTs-2017, and BraTs-2018, respectively. Özyurt et al. [27] presented a technique for detecting brain tumors. They began with MRI tumor image segmentation with the NS-EMFSE algorithm. They obtained features from the segmented image using AlexNet and then using the SVM, they detected and classified brain tumor images as benign or malignant, with 95.62 % accuracy.

However, most of these models are assessed on small-scale datasets due to the inaccessibility of the data repositories. Likewise, the majority of earlier research was based on pre-trained CNN models which were developed generally for a dataset of natural images. Pretrained models are customized for the brain tumor task without designing them to distinguish brain tumor patterns. Thus it limits the use of pre-trained CNN models for brain tumor diagnosis.

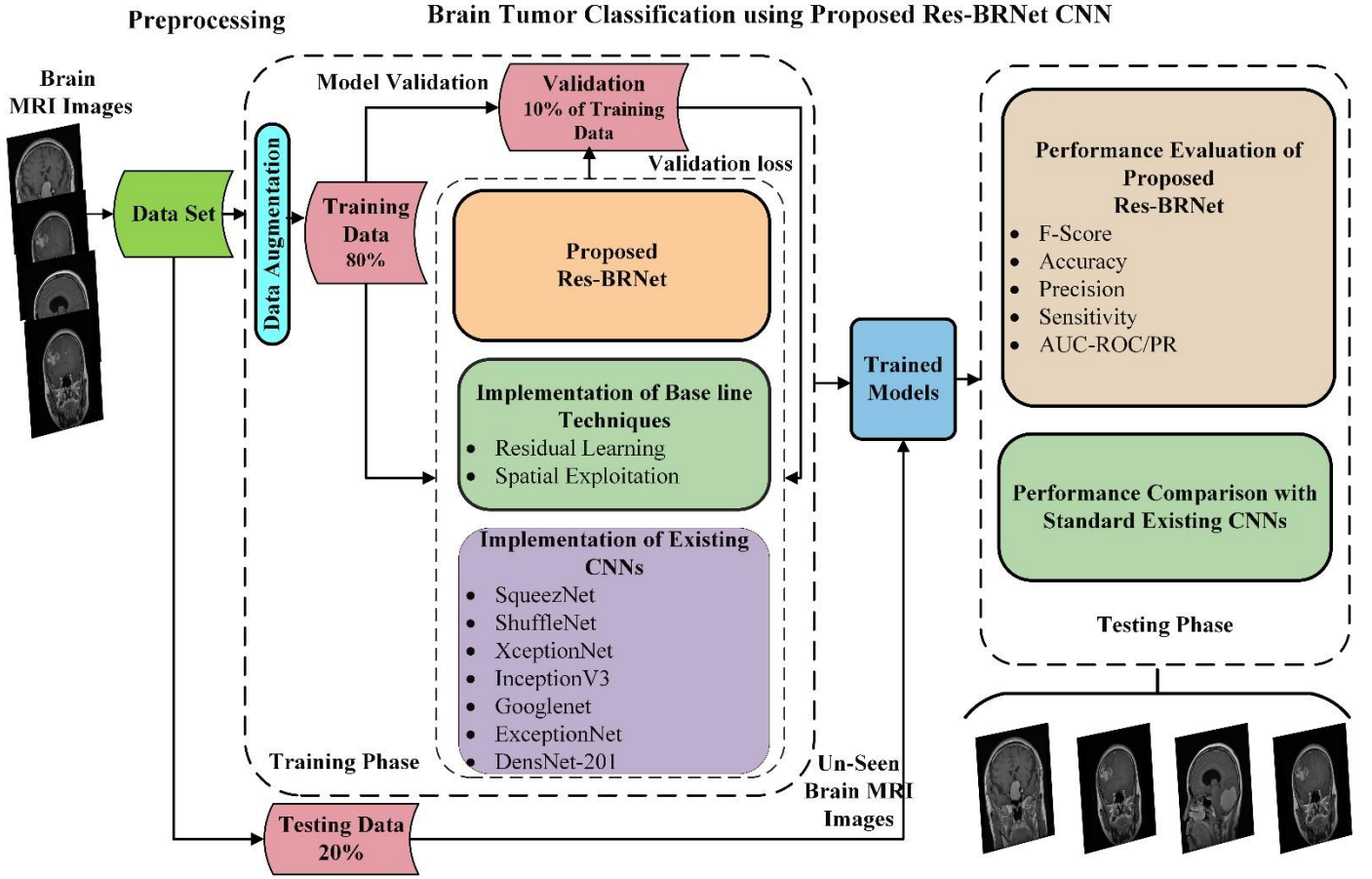
---

In this study, a new deep CNN-based brain tumor classification scheme is developed for MRI image categorizing. Performance assessment is performed using standard measures like sensitivity, precision, F\_score, accuracy, and AUC-PR/ROC. Moreover, we have generated a large dataset by collecting brain MRI images of three tumor types and normal brain images from publicly accessible sources. A novel CNN architecture, Res-BRNet, is suggested for brain tumor classification. The prediction ability of the developed approach is assessed on the test dataset and evaluated by comparing numerous existing DCNNs, and also proposed technique's idea is compared with baseline approaches. The proposed work has the following contributions:

- A new deep residual and regional CNN architecture, Res-BRNet, is developed for brain tumor classification.
- The developed Res-BRNet employed Regional and boundary-based operations in a systematic order within the modified spatial and residual blocks to exploit spatial correlation information and textural variations from brain tumor MRIs.
- The systematic integration of residual and spatial blocks within the proposed Res-BRNet CNN improves discriminative capability and generalization. Moreover, spatial blocks extract homogeneity and boundary-defined features at the abstract level. Furthermore, residual blocks at the target level significantly learn local and global texture variations of different classes of brain tumors.
- The proposed brain tumor Res-BRNet classification CNN significantly reduces false positives and negatives compared to several existing CNN architectures.

## 2. Methodology

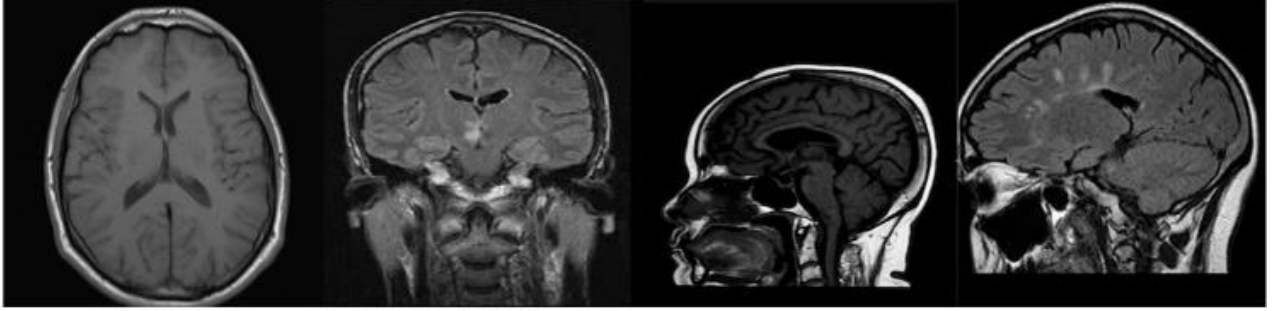
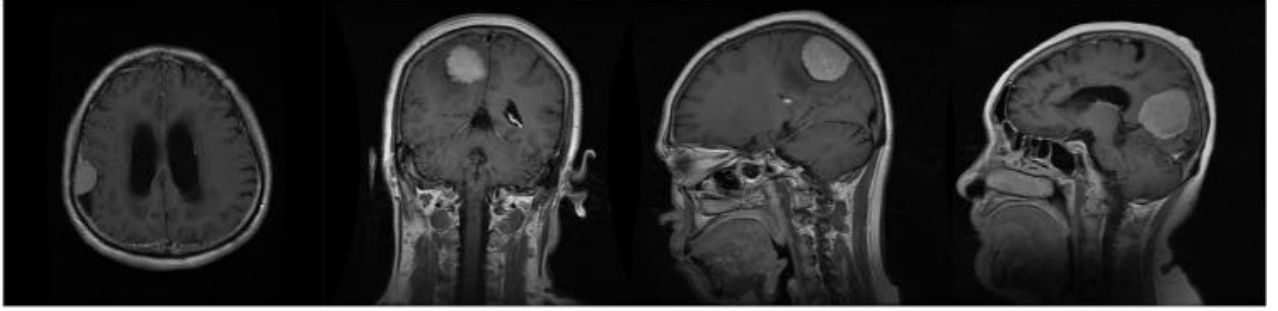
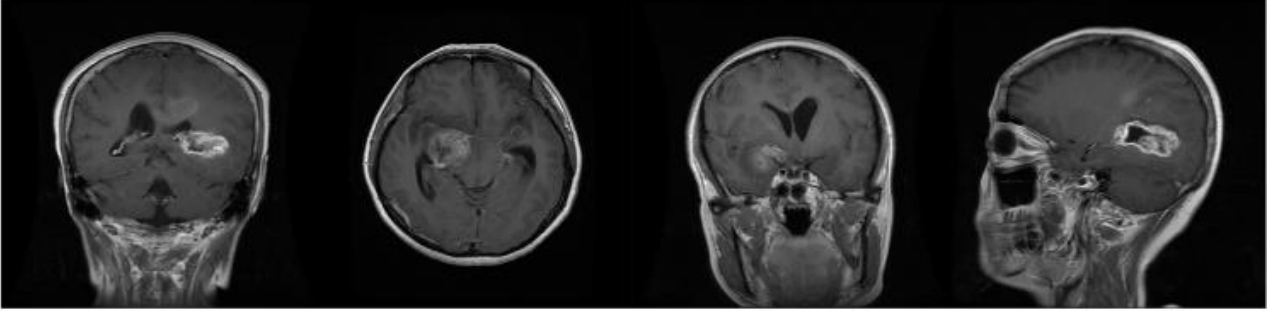
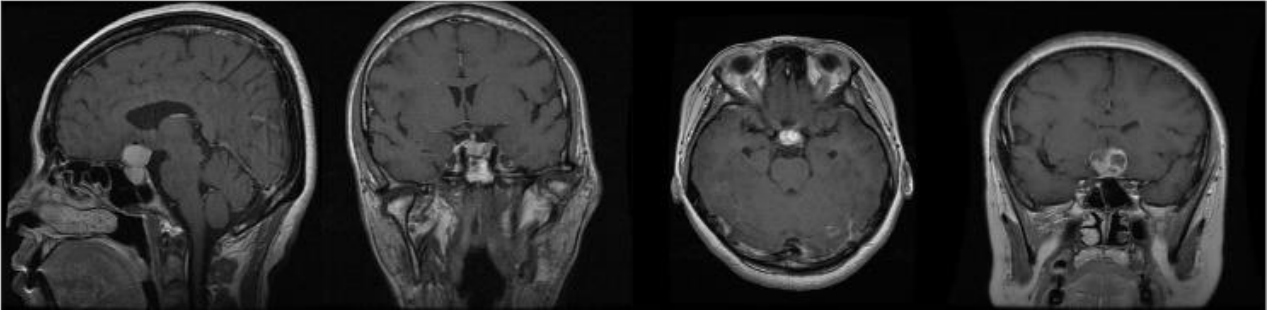
A novel deep residual and regional CNN architecture is designed for this study for automated brain tumors classification from MRI images. The suggested classification technique's discriminating ability is empirically assessed using several measures, and results are evaluated by comparing them with existing DCNNs. A better generalization is achieved by augmenting the training samples in the experimental setup. The general framework of the developed brain tumor classification technique is shown in Fig. 1.



**Figure 1.** The detailed design of the proposed brain tumor MRI images classification technique

## 2.1. Data Set

In this model, we formed a dataset containing MRI images of healthy individuals and three distinct types of brain tumors. MRI scans of four classes were gathered from Open Source Kaggle repositories [28], Br35H [29], and figshare [30]. For this experimental setup, we collected 2044 brain normal, 2352 glioma\_tumor, 1645 meningioma\_tumor, and 1831 pituitary\_tumor MRI images from these repositories; hence, in nature, the acquired dataset is unbalanced. Each image was resized to  $227 \times 227$  pixels. Some of the four classes' images are displayed in Fig. 2.

**A****B****C****D**

**Figure 2.** Example MRI images of normal and different types of tumors (A) Normal, (B) Glioma\_tumor, (C) Meningioma\_tumor, and (D) Pituitary\_tumor

## 2.1. Data Augmentation

On a small volume of data, deep learning models generally overfit. Thus, a significant amount of data is usually required to train deep CNNs and to provide better generalizability. Data augmentation implies increasing the original dataset's samples [6], [31], [32]. In this experiment, random rotation (0 - 360 degrees), scaling (0.5 - 1), shearing ( $\pm 0.05$ ), and image reflecting ( $\pm 1$  range) are used to augment the data set. These augmentation techniques are used to increase the model's generalization.

## 2.2. The developed deep Res-BRNet-based categorization

In this work, we exploit the learning capability of deep CNN to acquire the tumor's distinctive patterns in brain MRI images. The strong potential of deep CNN for learning specific features and patterns from images inspires their implementation for classification and recognition tasks. Because of their effective learning capability, CNNs are largely employed for feature extraction and classification. In this proposed work, we designed a novel residual and regional CNN architecture using boundary and Region-based operations to classify tumor-specific abnormalities in brain MRI images and named it Res-BRNet. The proposed model is trained in an end-to-end way to learn the tumor-related patterns from MRI scans. The last fully connected layers, followed by softmax-based operation of the proposed deep CNNs, is used for the final classifications. The details of Res-BRNet are described in the section given below.

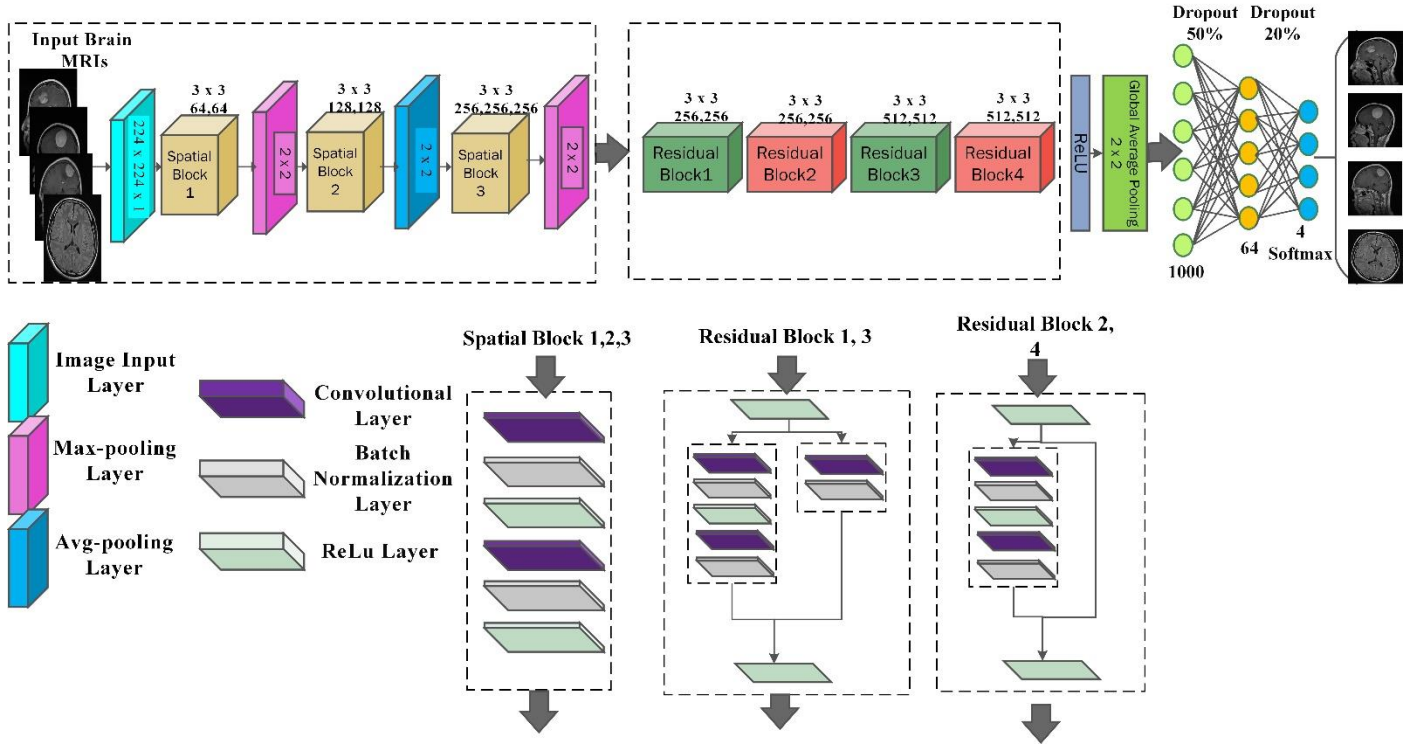


Figure 3. Blockwise details of the proposed Res-BRNet

### 2.2.1. Structural details of the developed Res-BRNet

The architecture-level details of the developed Res-BRNet are inspired by standard image processing techniques [33][34]. It is developed to explore the hidden insights in MRI images. In this context, the region and edge-based operators with convolution operators are optimized in the proposed architecture to attain the brain tumor patterns excellently. In this work, we exploited spatial and Residual blocks [35]–[37] as

baselines to justify the advantages of boundary uniformity and Edge-related concept for obtaining the patterns using CNNs.

As illustrated in Fig. 4 in spatial block, input  $x$  is fed into operation block and all operators are applied sequentially on input and at the output of operation block we get  $f(x)$  as shown in Eq. 1. Difference between a spatial and residual block is that residual contains a short path from input  $x$  to output block and ignore in between operations and add up with the output  $f(x)$  of encoding block and get  $f(x) + x$  as shown in Eq. 2. As compared to spatial block, residual block learning facilitates for vanishing gradient issue and as well as improves the feature maps and convergence.

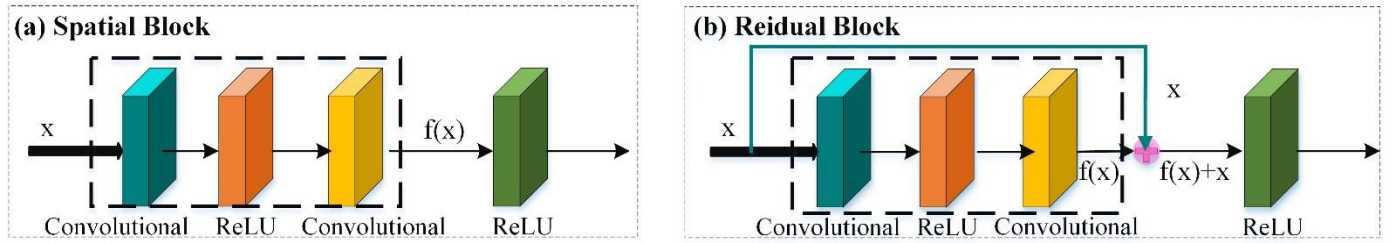


**Figure 4.** The difference in the process of (a) plain and (b) residual block

The proposed Res-BRNet comprises three spatial blocks at the start, and four residual blocks are used after them. Every spatial block contains a single convolution layer (Eq.3), batch normalization, and ReLU. The convolution-layer exploits tumor-relating patterns, while ReLU performs as an activation function. To learn region homogeneity and edge-related attributes of brain tumors, a max- or average-pooling operation is applied to the end of each spatial block, as shown in Equations (4) and (5).

Fig. 3 shows the architecture of the developed Res-BRNet. Fully connected (FC) layers stated in Eq. (6) are applied in the designed architecture to attain particular attributes for classification. Dropout layers are used with FC layers to minimize the risks of overfitting.

$$T(x) = F(x) \quad (1)$$

$$T(x) = F(x) + x \quad (2)$$

$$Z_{m,n} = \sum_{u=1}^r \sum_{v=1}^s Z_{m+u-1, n+v-1} k_{a,b} \quad (3)$$

$$Z_{m,n}^{Avg} = \frac{1}{T^2} \sum_{u=1}^t \sum_{v=1}^t Z_{m+u-1, n+v-1} \quad (4)$$

$$Z_{m,n}^{Max} = \text{Max}_{u=1 \dots t, v=1 \dots t} Z_{m+u-1, n+v-1} \quad (5)$$



---


$$Q = \sum_b^B \sum_c^C W_d Z_c \quad (6)$$

$Z$  illustrates the source feature map of size  $M \times N$ , and the filter with size  $r \times s$  is defined by  $k$  in the convolutional operator used in Equation (2). The output map of features is shown by  $Z$ .  $m$  and  $n$  have begun from 1 to  $(M - r + 1)$  and  $(N - s + 1)$ , accordingly. As shown in Equations (3)–(5), we regulate the  $Z_{avg}$  and  $Z_{max}$  methods, denoted by  $Z_{Avg}$  and  $Z_{Max}$ , similarly. In Equations (4) and (5),  $t$  indicates the average- and max-window dimensions. In Equation (6), the dense layer outcome is stated by  $Q$ , which employs global operation on  $Z_c$ . FC-layers neurons are presented by  $W_d$  and preserves essential features for the analysis.

### 2.2.2. Benefits of the proposed Res-BRNet for image contents analysis

Brain MRI scans reveal complex patterns with different levels of intensity which vary in different regions. Regional softness, textural differences, and edges make up these patterns' basic structure. In this study, the developed models are significantly improved by combining the convolutional operator (Eq. 3)), enhancing the region-homogeneity, and boundary-based operations (Eqs. (4) and ((5)), respectively, to differentiate the healthy instances from the tumor-affected MRI scans. In comparison to this method, the majority of existing CNN designs employ different convolutional combinations with simply the pooling layers to capture invariant features [36], [38]–[42]. The following are the significance of applying the developed idea in CNN:

- The developed residual and regional CNN architecture aimed to exploit image smoothness and sharpness dynamically, and it may effectively optimize the level of smoothness and sharpening in harmony with the spatial features of an image.
- Implementation of the spatial block (Eq. (1)) with residual learning improves the overall detection ability of the model by acquiring textural features along with spatial correlation from MRI images.
- Residual blocks (Eq. (2)) facilitate the model to resolve the vanishing gradient problem, which is generally produced in very deep architectures.
- The systematic use of boundary and regional operations within spatial blocks helps enhance the region homogeneity of various regions. Using average-pooling (Eq. (4)), the region operator helps smooth the regional variations and eliminates noise caused by distortions captured during MRI imaging. On the

---

other hand, CNN is encouraged by edge operators to acquire discriminating local features with the max-pooling operation (Eq. (5)).

- Down-sampling is also performed during pooling operations, which increases the model's robustness to small changes in the input image.

### **2.3. Employment of Existing CNNs**

Competitive assessment is performed by implementing several existing deep CNN models, including SqueezeNet, ShuffleNet, VGG-16, Xception, ResNet-18, GoogleNet, Inception-V3, and DenseNet-201 [36], [39], [40], [42]–[47]. Several researchers applied these CNNs for the classification of MRI images, and they have been widely used for a number of image recognition tasks. Although these models' block architecture and design changed, they all employed a single pooling operation along the network or changed this out for a stridden convolution operation to control complexity. In order to fine-tune these CNNs for brain tumor classification, we added FC as well as a classification layer and employed them in an end-to-end manner.

### **2.4. Implementation details**

A brain MRI dataset was split into two sets, 80% train set, and 20% test set. Furthermore, the train set was divided into train and validation data to select optimized parameters. 'RMSprop' [48] was employed for optimization with a 'SquaredGradientDecayFactor' of 0.95 throughout the training of CNNs. The learning rate was initially set to 0.0001 with the "LearnRateDropFactor" to be 0.4, and epochs 40. A small-batch-based technique is used to train models on batch size=16 for every epoch. As an activation function Softmax was used, and cross-entropy loss has been reduced for all of the deep CNNs optimizations. This simulation was conducted using MATLAB 2020b. During MATLAB-based simulations, a 2.90-GHz Dell, Core I i7-7500 CPU and a Nvidia® GTX 1060 Tesla graphics card with CUDA support have been used.

## **3. Results and discussion**

This study suggests a deep CNN-based scheme for identifying brain tumor patients using brain MRI images. We perform two different experiments for empirical evaluation of the developed method. We initially explore the impacts of using simultaneously average- and max-pooling in spatial and residual blocks of Res-BRNet. Secondly, a general assessment of brain tumor classification is carried out by comparing performances with well-known existing methods.

---

### 3.1. Performance metrics

The efficiency of the developed model is assessed using several standard evaluation measures. These measures include precision [49], sensitivity [50], accuracy [51], F-score [52], and ROC curve [53]. TP defined truly positive predictions, TN as truly negative predictions, FP as incorrectly positive predictions, and FN for incorrectly negative predictions. In (Eq. (5)) accuracy is defined, it calculates the total number of accurate selections. Accordingly, Sensitivity is in (Eq. (6)), precision is denoted in (Eq. (7)), and F-score is defined in (Eq. (8)).

$$\text{Acc} = \left( \frac{\text{TP} + \text{TN}}{\text{TN} + \text{TP} + \text{FN} + \text{FP}} \right) \times 100 \quad 5)$$

$$\text{Sensitivity} = \frac{\text{TP}}{\text{TP} + \text{FN}} \quad 6)$$

$$\text{Precision} = \frac{\text{TN}}{\text{TN} + \text{FP}} \quad 7)$$

$$\text{F1\_Score} = \frac{2 \times (\text{P} \times \text{R})}{\text{P} + \text{R}} \quad 8)$$

### 3.2. Efficiency analysis of the proposed Res-BRNet

The proficiency of the developed Res-BRNet is validated on unseen test data primarily focused on standard measures and accuracy. In contrast to Accuracy, F-score tends to give more weight to precision and sensitivity. Training-loss and accuracy chart for Res-BRNet is presented in Fig. 5. The designed CNN's converge smoothly and quickly to achieve their optimal value, as seen in the accuracy and loss chart (Fig. 5). The proposed Res-BRNet model correctly classified 1546 samples of three brain tumors and normal instances. Likewise, the proposed Res-BRNet performs similarly by correctly identifying 463 gliomas, 321 meningiomas, 365 pituitary, and 404 normal individuals correspondingly. It is observed that a change in the region and boundary arrangements, as illustrated in Fig.3, improves the overall performance. Fig. 5 displays some of the brain MRI images that Res-BRNet misclassifies. Low contrast, irregular sample patterns, and varying illumination variations are probable reasons for misclassification. The generalization and the robustness enhancement of test samples, is achieved by using several data-augmentation strategies while train developed CNNs.

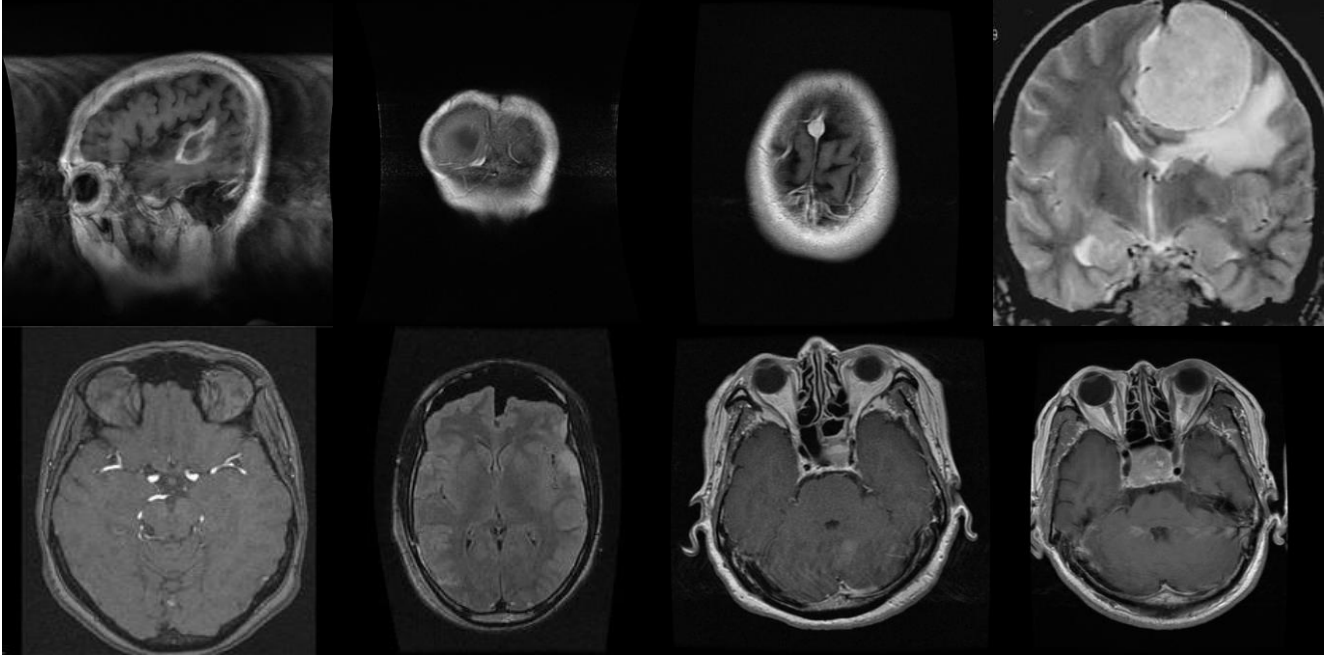


**Figure 5.** Normal and three tumor images that are misclassified by Res-BRNet

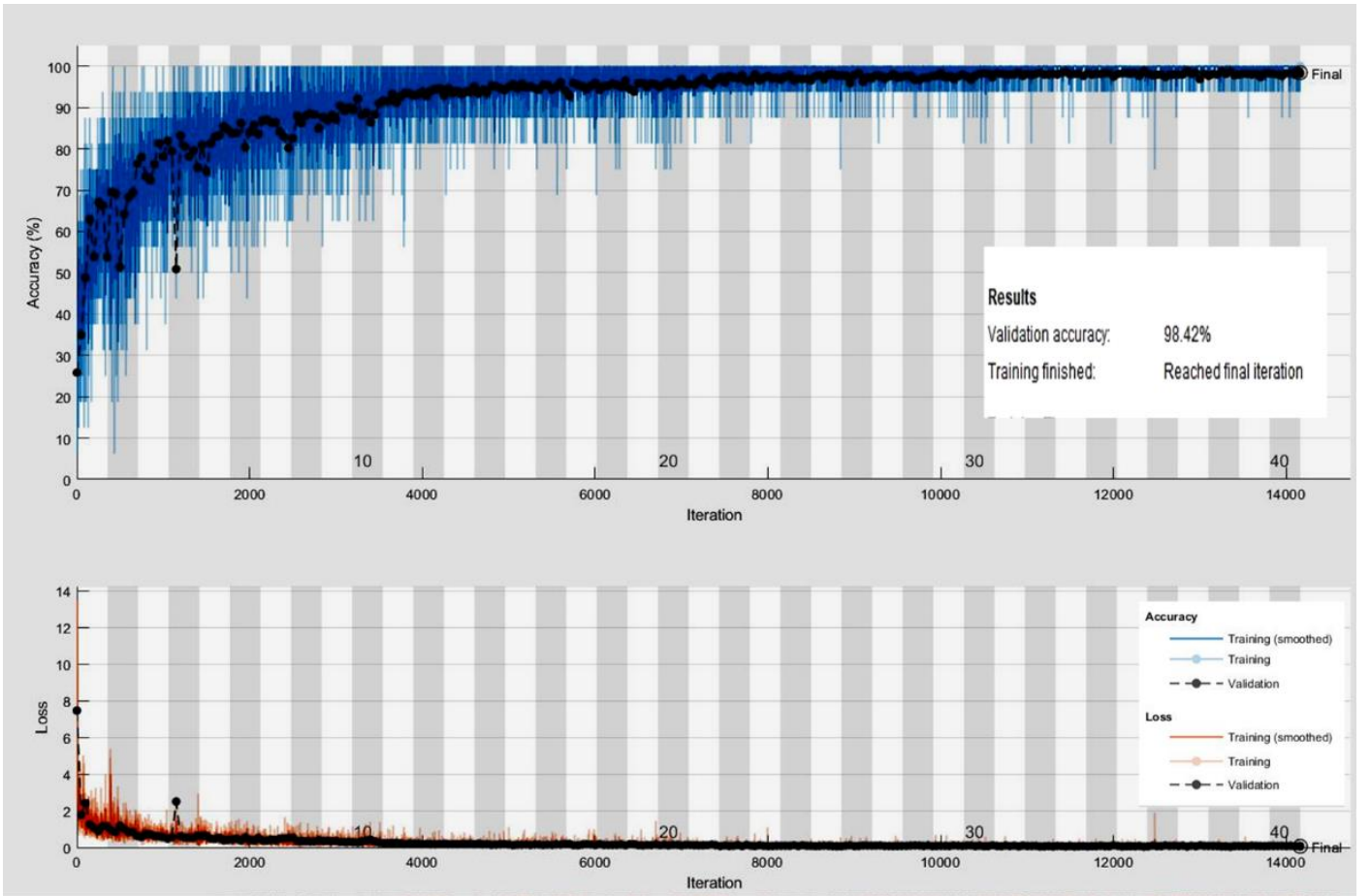


**Figure 6.** Plots for training the proposed Res-BRNet

### 3.2.1. Analysis of performance with base-line methods

The significance of the anticipated idea is assessed by evaluating the performance, especially in comparison to residual learning and spatial exploitation-based architectures. Both baseline

architectures, VGG-16 and ResNet-18 are almost deep as Res-BRNet. Spatial block-based architectures exploit one type of down-sampling operation, and residual blocks use stridden convolution instead of pooling down in contrast, employing both pooling operators in Res-BRNet improves the overall performance as shown in Table 2. Thus, according to performance comparison, the Res-BRNet shows exceptional performance as compared to residual blocks and Spatial block-based architectures in terms of F-score (0.9641) and accuracy of (98.22%).

**Table 1.** Performance evaluation of the developed Res-BRNet with baseline architectures using the test data.

Model	Performance comparison with custom-made CNNs			
	Accuracy %	Sensitivity	Precision.	F1-Score
VGG-16	93.32	0.9285	0.8231	0.8719
TL_VGG-16	94.66	0.9426	0.8569	0.8961
ResNet-18	95.67	0.9566	0.8788	0.9158
TL_ResNet-18	96.44	0.9641	0.8998	0.9303
<b>Proposed Res-BRNet</b>	<b>98.22</b>	<b>0.9811</b>	<b>0.9822</b>	<b>0.9641</b>

**Fig. 7.** shows that the suggested Res-BRNet considerably enhances the detection ability for all three brain tumors as well as for normal MRI images compared to baseline residual learning and spatial exploitation architectures.

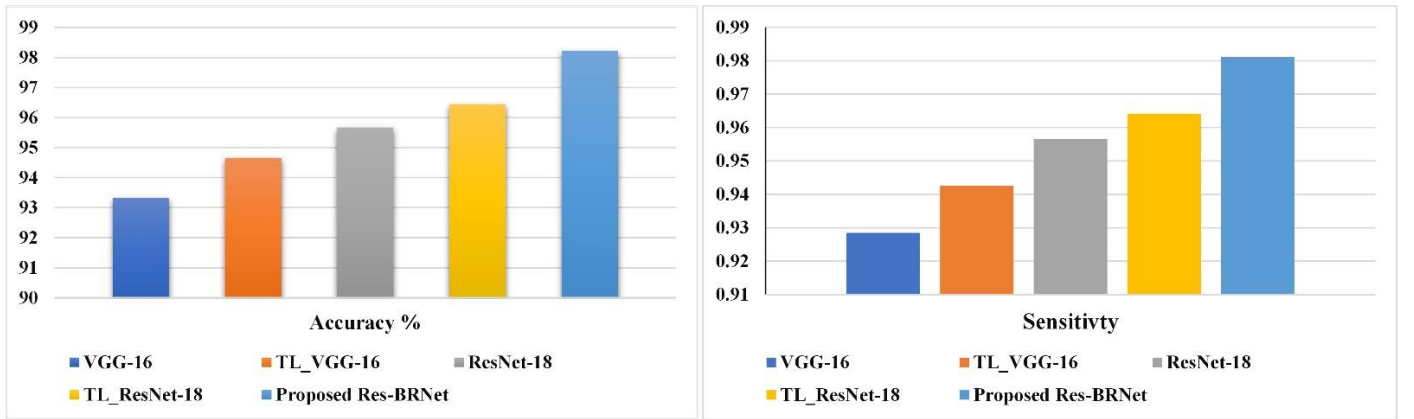


**Figure 7.** Performance assessment of the developed Res-BRNet with baseline architectures

### 3.2.2. Feature space-based Performance Analysis

In order to understand decision-making behaviour, the proposed Res-BRNet and best-performing baseline architectures, ResNet-19 and VGG-16 are evaluated to examine the feature space they learn. Characteristics of the feature space responsible for the discrimination capability of a classifier. Features with classes distinguishably improve the model's learning and lower the variance on distinct samples. T-distributed Stochastic Neighbor Embedding (t-SNE) [54] is an algorithm that is well-suited to visualize by embedding high-dimensional points in low dimensions based on similarities between points. Fig.8 illustrate

the 2-D t-SNE plots for the proposed Res-BRNet, ResNet-18 and VGG-16 using testing data. Data visualization shows that the feature space diversity is significantly improved by using both the max and average pooling operations, and improves classifier performance.

### 3.3. Detection abilities of the developed Res-BRNet

In a comprehensive experimental investigation, the proposed method is assessed with well-known CNNs on unseen brain MRI images for performance evaluation using Accuracy, F-score, Sensitivity, and Precision.

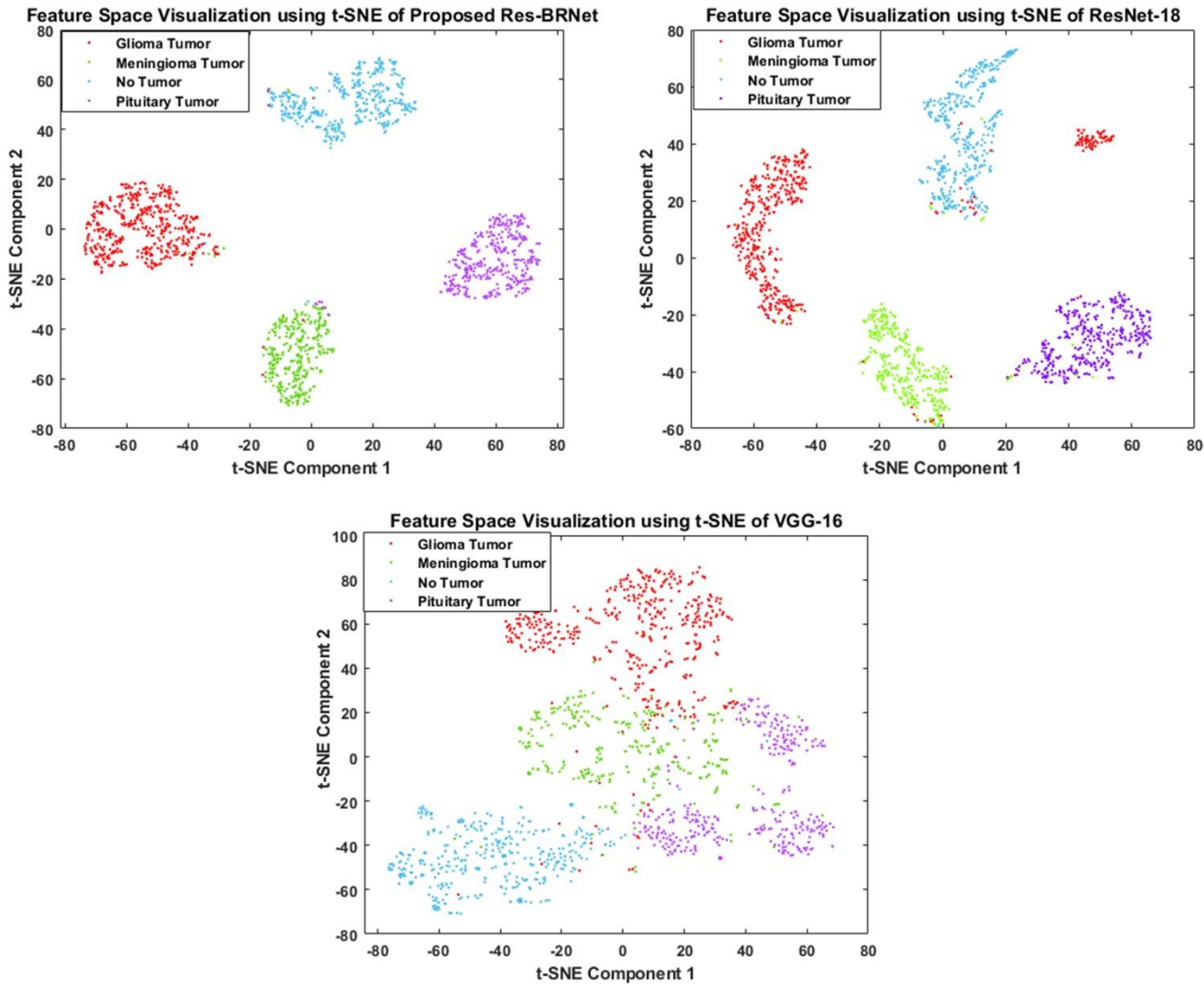


**Figure 8.** Feature space-based performance analysis of the developed Res-BRNet with baseline architectures

#### 3.3.1. Performance assessment with existing CNNs

The effectiveness of the developed Res-BRNet is compared with custom-made train-in-from-scratch and transfer learning-based (TL-based) existing CNNs, namely; SqueezeNet, ShuffleNet, VGG-16, Xception, ResNet-18, GoogleNet, InceptionV3, and DenseNet-201. Tables 2 and 3. illustrate that the proposed models' performance analysis indicates, Res-BRNet is more efficient at identifying the patterns

specific to the brain tumors in MRI scans with standard measures of accuracy and F-score. This performance of the proposed model has been improved by using average\_ and max\_pooling operations systematically in the designed CNN ( Fig. 9 and Tab. 4) . In general, the model is encouraged to learn highly discriminative features and fine-grained information from the raw MRI image by the use of these opposing pooling operations.

**Table 2.** Performance analysis of the existing standard custom CNNs and the proposed Res-BRNet on the testing data.

Model	Performance comparison with custom-made CNNs			
	Accuracy %	Sensitivity	Precision.	F1-Score
SqueezeNet	87.16	0.8691	0.6946	0.7671
ShuffleNet	89.45	0.8923	0.7411	0.8047
VGG-16	93.32	0.9285	0.8231	0.8719
Xception	95.36	0.9531	0.8721	0.9101
ResNet-18	95.67	0.9566	0.8788	0.9158
GoogleNet	95.87	0.9593	0.8851	0.9196
Inception-V3	96.56	0.9676	0.9015	0.9331
DenseNet-201	97.01	0.9668	0.9175	0.9406
<b>Proposed Res-BRNet</b>	<b>98.22</b>	<b>0.9811</b>	<b>0.9822</b>	<b>0.9641</b>

**Table 3.** Performance analysis of the existing standard TL-based CNNs and the proposed Res-BRNet on the testing data.

Model	Performance comparison with TL-Based CNNs			
	Accuracy %	Sensitivity	Precision.	F1-Score
TL_SqueezeNet	90.91	0.9108	0.7685	0.8315
TL_ShuffleNet	92.31	0.9155	0.8056	0.8521
TL_VGG-16	94.66	0.9426	0.8569	0.8961
TL_Xception	96.37	0.9611	0.8996	0.9285
TL_ResNet-18	96.44	0.9641	0.8998	0.9303
TL_GoogleNet	96.37	0.9641	0.8985	0.9291
TL_Inception-V3	97.26	0.9711	0.9225	0.9459
TL_DenseNet-201	97.77	0.9778	0.9349	0.9557
<b>Proposed Res-BRNet</b>	<b>98.22</b>	<b>0.9811</b>	<b>0.9822</b>	<b>0.9641</b>

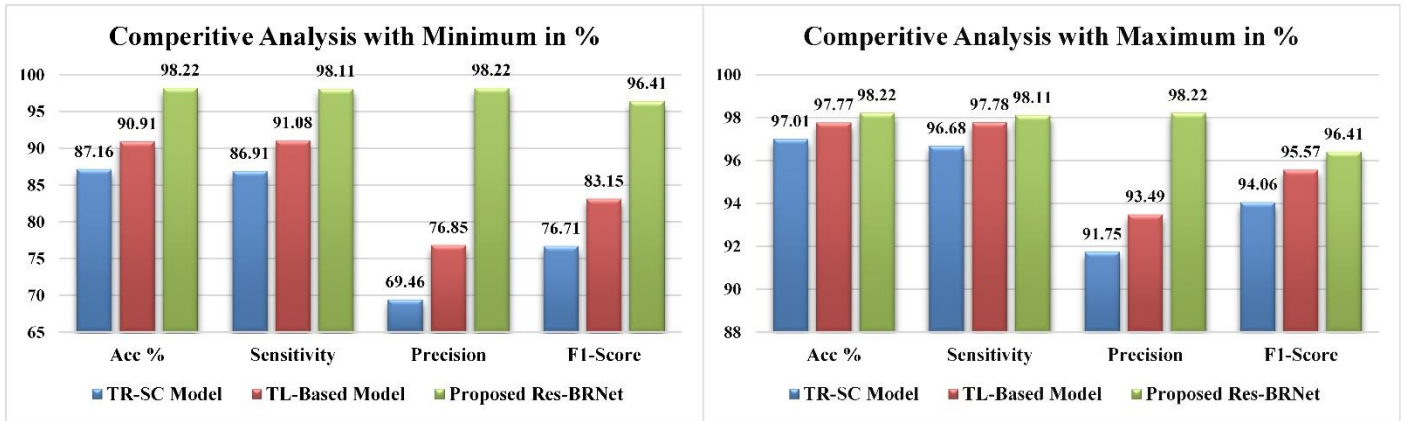


**Figure 9.** Performance improvement of the developed Res-BRNet

**Table 4** Performance improvement of the developed Res-BRNet as compare to TR-SC and TL-Based Models

	Improvmnts	Acc %	Sensitivity	Precision	F1-Score
1	TR-SC to TL-B	0.76 – 3.75 %	1.1 – 4.45 %	1.74 – 7.39 %	1.51 – 6.44 %
2	TR-SC to Proposed Res-BRNet	1.2 – 11.06 %	1.43 -11.02 %	6.47 – 28.76 %	2.35 – 19.07 %
3	TL-B to Proposed Res-BRNet	0.45 – 7.31 %	1.1 – 4.17 %	1.74 – 7.39 %	1.51 – 6.44 %

### 3.3.2. ROC and PR-AUC based analysis

The ROC curve is essential for the classifier to achieve the optimal analytic threshold. ROC curve displays the classifier distinction capability at possible threshold values graphically. As shown in Fig.10, the proposed Res-BRNet achieved an AUC of (0.9921 and 0.9702) on the brain MRI dataset. ROC and PR-AUC quantitative analysis prove that the suggested method enhances sensitivity by having the lowest false-positive rate. This shows that the presented approach for classifying brain tumors has a lot of potentials to be used in the analysis of brain tumors.

### 3.3.3. Screening effectiveness of the proposed technique

Precision and detection rate (sensitivity) are the primary metrics to evaluate a medical diagnostic system's efficiency. The brain tumor detection system needs to have a good detection performance. As can be seen in Fig. 10 and Table 2, the detection rate and precision of the proposed approach are evaluated for brain MRI images. As shown in the quantitative study (Fig. 11), the Res-BRNet (Sensitivity: 0.9811, Precision: 0.9822) increases the prediction system's accuracy and has a high prediction rate. Consequently, it is expected to help the radiologist with good accuracy and may be utilized to enhance efficiency by decreasing the burden.



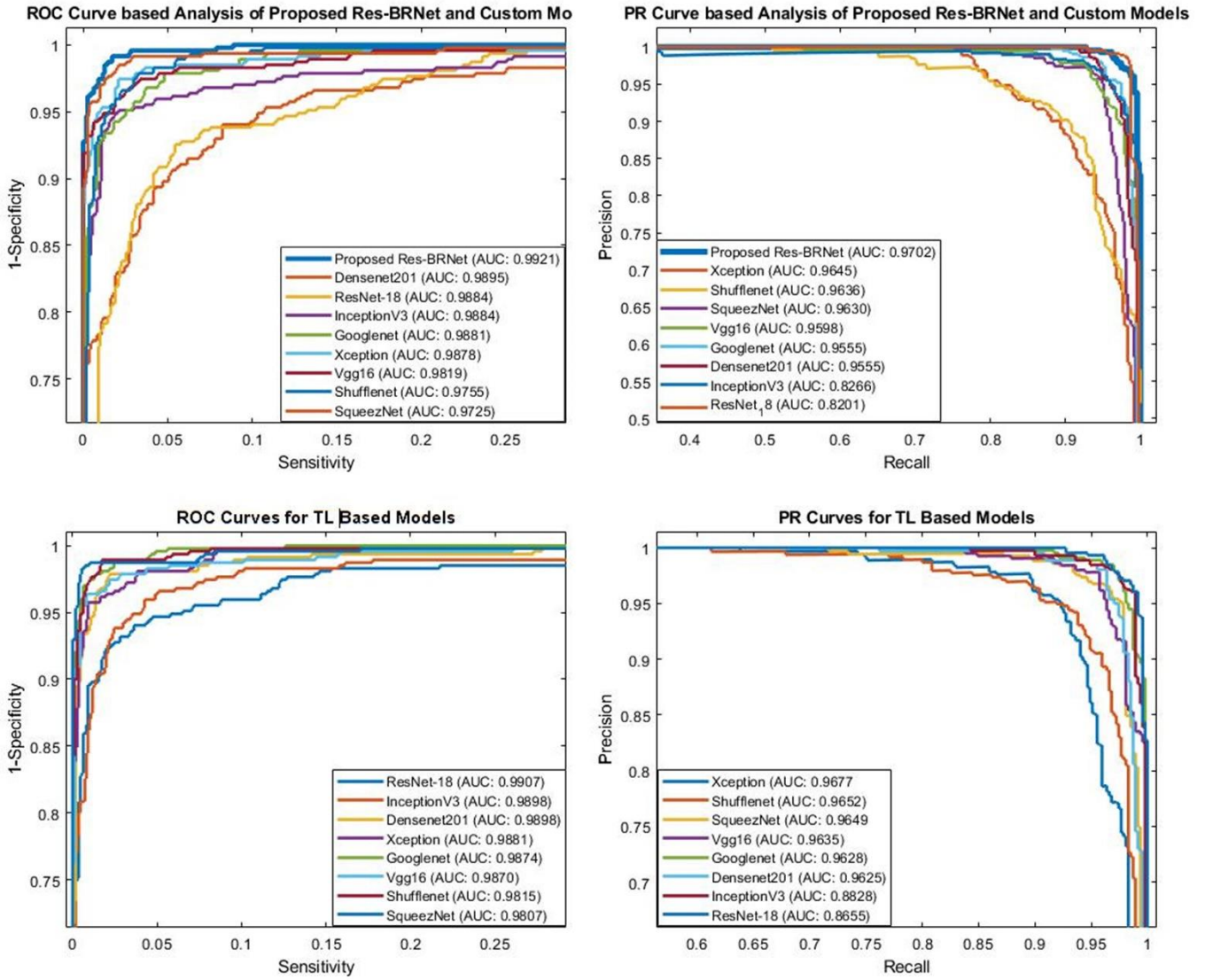


Figure 10. performance analysis of the developed Res-BRNet with existing CNNs

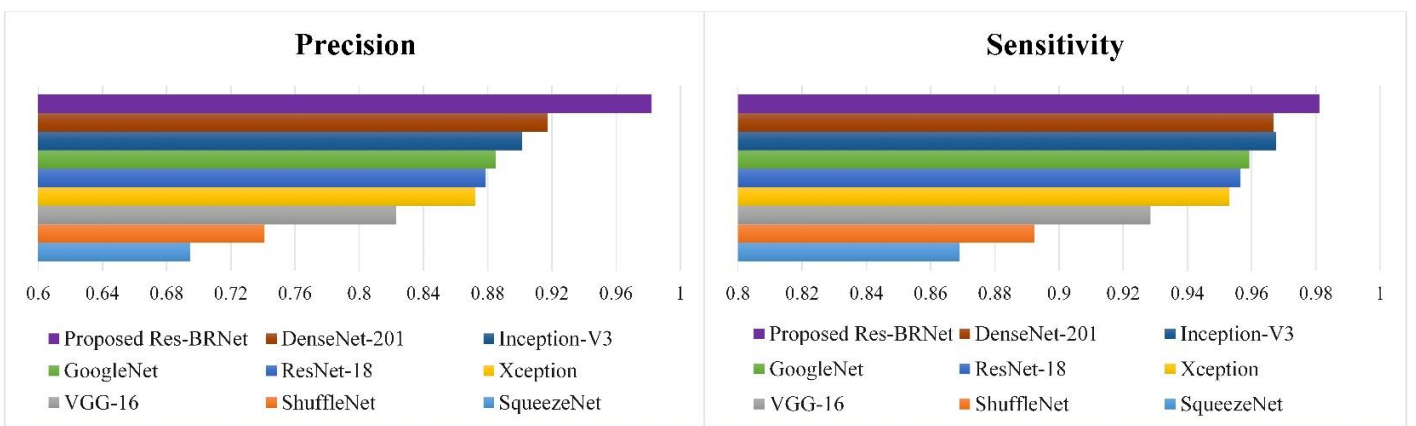


Figure 11. performance analysis of the developed Res-BRNet with existing CNNs

## 4. Conclusion

Brain tumor diagnosis at an early stage is crucial to cure the patient. Therefore, in this work, a new customized deep CNN model is developed to classify the brain MRI scans of meningioma-, glioma-, and pituitary-tumor from healthy entities. The performance exploration of the developed brain tumor

categorization system is analyzed with the existent Deep CNN models. The experiment results show that the proposed Res-BRNet outperforms existing CNN architectures, indicating accuracy and F-score improvement. The developed method classifies brain tumors with an accuracy of 98.22%, an F1-Score of 0.9641 with sensitivity and precision of 0.9811 and 0.9822 correspondingly. The proposed approach will likely facilitate healthcare professionals in making diagnoses of brain tumors. Additionally, It motivates to be used in exploring different forms of abnormalities in brain MRI images.

## References

- [1] A. Behin, K. Hoang-Xuan, A. F. Carpentier, and J.-Y. %J T. L. Delattre, "Primary brain tumours in adults," *Lancet*, vol. 361, no. 9354, pp. 323–331, 2003.
- [2] K. D. Miller *et al.*, "Brain and other central nervous system tumor statistics, 2021," *CA. Cancer J. Clin.*, vol. 71, no. 5, pp. 381–406, Sep. 2021, doi: 10.3322/caac.21693.
- [3] "Brain and Spinal Cord Tumors in Adults." <https://www.cancer.org/cancer/brain-spinal-cord-tumors-adults.html> (accessed Aug. 18, 2022).
- [4] E. A. S. El-Dahshan, H. M. Mohsen, K. Revett, and A. B. M. Salem, "Computer-aided diagnosis of human brain tumor through MRI: A survey and a new algorithm," *Expert Syst. Appl.*, vol. 41, no. 11, pp. 5526–5545, 2014, doi: 10.1016/j.eswa.2014.01.021.
- [5] K. M. Iftexharuddin, J. Zheng, M. A. Islam, and R. J. Ogg, "Fractal-based brain tumor detection in multimodal MRI," *Appl. Math. Comput.*, vol. 207, no. 1, pp. 23–41, 2009, doi: 10.1016/j.amc.2007.10.063.
- [6] M. M. Zahoor *et al.*, "A New Deep Hybrid Boosted and Ensemble Learning-Based Brain Tumor Analysis Using MRI," *Sensors 2022, Vol. 22, Page 2726*, vol. 22, no. 7, p. 2726, Apr. 2022, doi: 10.3390/S22072726.
- [7] A. Khan, S. H. Khan, M. Saif, A. Batool, A. Sohail, and M. W. Khan, "A Survey of Deep Learning Techniques for the Analysis of COVID-19 and their usability for Detecting Omicron," *arXiv Prepr. arXiv2202.06372*, Feb. 2022, Accessed: Aug. 01, 2022. [Online]. Available: <http://arxiv.org/abs/2202.06372>
- [8] S. H. Khan, A. Sohail, A. Khan, and Y. S. Lee, "Classification and Region Analysis of COVID-19 Infection using Lung CT Images and Deep Convolutional Neural Networks," Sep. 2020.
- [9] M. Asam *et al.*, "Detection of Exceptional Malware Variants Using Deep Boosted Feature Spaces and Machine Learning," *Appl. Sci.*, vol. 11, no. 21, p. 10464, 2021.
- [10] M. M. Zahoor, S. A. Qureshi, A. Khan, A. ul Rehman, and M. Rafique, "A novel dual-channel brain tumor detection system for MR images using dynamic and static features with conventional machine learning techniques," <https://doi.org/10.1080/17455030.2022.2070683>, 2022, doi: 10.1080/17455030.2022.2070683.
- [11] S. H. Khan, A. Sohail, and A. Khan, "COVID-19 Detection in Chest X-Ray Images using a New Channel Boosted CNN," *arXiv*. 2020.

- 
- [12] A. Alqahtani *et al.*, “Computer Aided COVID-19 Diagnosis in Pandemic Era Using CNN in Chest X-ray Images,” *Life* 2022, Vol. 12, Page 1709, vol. 12, no. 11, p. 1709, Oct. 2022, doi: 10.3390/LIFE12111709.
- [13] Z. Akkus, A. Galimzianova, A. Hoogi, D. L. Rubin, and B. J. Erickson, “Deep learning for brain MRI segmentation: state of the art and future directions,” *J. Digit. Imaging*, vol. 30, no. 4, pp. 449–1889, 2017.
- [14] I. Domingues, G. Pereira, P. Martins, H. Duarte, J. Santos, and P. H. Abreu, “Using deep learning techniques in medical imaging: a systematic review of applications on CT and PET,” *Artif. Intell. Rev.*, 2020, doi: 10.1007/s10462-019-09788-3.
- [15] C. A. Goodfellow Ian, Bengio Yoshua, “Deep Learning - Ian Goodfellow, Yoshua Bengio, Aaron Courville - Google Books,” *MIT Press*. p. 800, 2016.
- [16] W. Gómez-Flores *et al.*, “A comparative study of pre-trained convolutional neural networks for semantic segmentation of breast tumors in ultrasound,” *Comput. Biol. Med.*, vol. 126, no. January, pp. 2419–2428, Jun. 2020, doi: 10.1016/j.compbimed.2020.104036.
- [17] W. Rawat and Z. Wang, “Deep convolutional neural networks for image classification: A comprehensive review,” *Neural Comput.*, vol. 29, no. 9, pp. 2352–2449, Sep. 2017, doi: 10.1162/NECO\_A\_00990.
- [18] M. Arabahmadi, R. Farahbakhsh, and J. Rezazadeh, “Deep Learning for Smart Healthcare—A Survey on Brain Tumor Detection from Medical Imaging,” *Sensors* 2022, Vol. 22, Page 1960, vol. 22, no. 5, p. 1960, Mar. 2022, doi: 10.3390/S22051960.
- [19] A. Z. Shirazi *et al.*, “The Application of Deep Convolutional Neural Networks to Brain Cancer Images: A Survey,” *J. Pers. Med.* 2020, Vol. 10, Page 224, vol. 10, no. 4, p. 224, Nov. 2020, doi: 10.3390/JPM10040224.
- [20] P. Papanagiotou *et al.*, “Convolutional Neural Network Techniques for Brain Tumor Classification (from 2015 to 2022): Review, Challenges, and Future Perspectives,” *Diagnostics* 2022, Vol. 12, Page 1850, vol. 12, no. 8, p. 1850, Jul. 2022, doi: 10.3390/DIAGNOSTICS12081850.
- [21] J. S. Paul, A. J. Plassard, B. A. Landman, and D. Fabbri, “Deep learning for brain tumor classification,” *Med. Imaging 2017 Biomed. Appl. Mol. Struct. Funct. Imaging*, vol. 10137, p. 1013710, Mar. 2017, doi: 10.1117/12.2254195.
- [22] S. Deepak and P. M. Ameer, “Brain tumor classification using deep CNN features via transfer learning,” *Comput. Biol. Med.*, vol. 111, pp. 103345 % @ 0010–4825, 2019.
- [23] A. Çinar and M. Yildirim, “Detection of tumors on brain MRI images using the hybrid convolutional neural network architecture,” *Med. Hypotheses*, vol. 139, Jun. 2020, doi: 10.1016/j.mehy.2020.109684.
- [24] H. H. Sultan, N. M. Salem, and W. Al-Atabany, “Multi-Classification of Brain Tumor Images Using Deep Neural Network,” *IEEE Access*, vol. 7, pp. 63536–69215, 2019.
- [25] S. Khawaldeh, U. Pervaiz, A. Rafiq, and R. S. Alkhawaldeh, “Noninvasive grading of glioma tumor using magnetic resonance imaging with convolutional neural networks,” *Appl. Sci.*, vol. 8, no. 1, p.

---

27, 2018.

- [26] M. A. Khan *et al.*, “Multimodal Brain Tumor Classification Using Deep Learning and Robust Feature Selection: A Machine Learning Application for Radiologists,” *Diagnostics (Basel, Switzerland)*, vol. 10, no. 8, p. 565, 2020, doi: 10.3390/diagnostics10080565.
- [27] F. Özyurt, E. Sert, E. Avci, and E. Dogantekin, “Brain tumor detection based on Convolutional Neural Network with neutrosophic expert maximum fuzzy sure entropy,” *Measurement*, vol. 147, p. 106830, Dec. 2019, doi: 10.1016/J.MEASUREMENT.2019.07.058.
- [28] “Br35H :: Brain Tumor Detection 2020 | Kaggle.”
- [29] “Brain Tumor Classification (MRI) | Kaggle.”
- [30] C. Jun, “brain tumor dataset %U [https://figshare.com/articles/brain\\_tumor\\_dataset/1512427](https://figshare.com/articles/brain_tumor_dataset/1512427).” 2017. doi: 10.6084/m9.figshare.1512427.v5     <https://ndownloader.figshare.com/files/3381290>     %2  
<https://ndownloader.figshare.com/files/3381293>     %2  
<https://ndownloader.figshare.com/files/3381296>     %2  
<https://ndownloader.figshare.com/files/3381302>     %2  
<https://ndownloader.figshare.com/files/7005344> %2 <https://ndownloader.figshare.com/files/7953679>.
- [31] C. Shorten and T. M. Khoshgoftaar, “A survey on Image Data Augmentation for Deep Learning,” *J. Big Data*, vol. 6, no. 1, p. 60, Dec. 2019, doi: 10.1186/s40537-019-0197-0.
- [32] A. Khan, A. Sohail, U. Zahoor, and A. S. Qureshi, “A survey of the recent architectures of deep convolutional neural networks,” *Artif. Intell. Rev.*, pp. 1–68, Apr. 2020, doi: 10.1007/s10462-020-09825-6.
- [33] S. Hussain and A. Khan, “Coronavirus Disease Analysis using Chest X-ray Images and a Novel Deep Convolutional Neural Network,” *10.13140/Rg.2.2.35868.64646*, no. April. pp. 1–31, 2020.
- [34] A. Mallick, S. Roy, S. S. Chaudhuri, and S. Roy, “Optimization of Laplace of Gaussian (LoG) filter for enhanced edge detection: A new approach,” *International Conference on Control, Instrumentation, Energy and Communication, CIEC 2014*. pp. 658–661, 2014. doi: 10.1109/CIEC.2014.6959172.
- [35] K. He, X. Zhang, S. Ren, and J. Sun, “Deep Residual Learning for Image Recognition,” *Proc. IEEE Comput. Soc. Conf. Comput. Vis. Pattern Recognit.*, vol. 2016-Decem, pp. 770–778, Dec. 2015, doi: 10.48550/arxiv.1512.03385.
- [36] K. Simonyan and A. Zisserman, “Very deep convolutional networks for large-scale image recognition,” *arXiv Prepr. arXiv1409.1556*, pp. 1–14, 2014.
- [37] S. H. Khan, N. S. Shah, R. Nuzhat, A. Majid, H. Alquhayz, and A. Khan, “Malaria parasite classification framework using a novel channel squeezed and boosted CNN,” *Reprod. Syst. Sex. Disord.*, vol. 71, no. 5, Oct. 2022, doi: 10.1093/JMICRO/DFAC027.
- [38] S. H. Khan, A. Khan, Y. S. Lee, and M. Hassan, “Segmentation of Shoulder Muscle MRI Using a New Region and Edge based Deep Auto-Encoder,” *arXiv Prepr. arXiv2108.11720*, 2021.
- [39] K. He, X. Zhang, S. Ren, and J. Sun, “Deep residual learning for image recognition,” *Proceedings of the IEEE Computer Society Conference on Computer Vision and Pattern Recognition*, vol. 2016-

- 
- Decem. pp. 770–778, 2016. doi: 10.1109/CVPR.2016.90.
- [40] G. Huang, Z. Liu, L. Van Der Maaten, and K. Q. Weinberger, “Densely connected convolutional networks,” *Proceedings - 30th IEEE Conference on Computer Vision and Pattern Recognition, CVPR 2017*, vol. 2017-Janua. pp. 2261–2269, 2017. doi: 10.1109/CVPR.2017.243.
- [41] S. Zagoruyko and N. Komodakis, “Wide Residual Networks,” *Proceedings Br. Mach. Vis. Conf. 2016*, pp. 87.1-87.12, May 2016, doi: 10.5244/C.30.87.
- [42] F. N. Iandola, M. W. Moskewicz, K. Ashraf, S. Han, W. J. Dally, and K. Keutzer, “SqueezeNet,” *arXiv*, 2016.
- [43] X. Zhang, X. Zhou, M. Lin, and J. Sun, “ShuffleNet: An Extremely Efficient Convolutional Neural Network for Mobile Devices,” 2018. doi: 10.1109/CVPR.2018.00716.
- [44] F. Chollet, “Xception: Deep learning with depthwise separable convolutions,” 2017, pp. 1251–1258.
- [45] C. Szegedy *et al.*, “Going deeper with convolutions,” 2015, pp. 1–9.
- [46] S. S. Yadav and S. M. Jadhav, “Deep convolutional neural network based medical image classification for disease diagnosis,” *J. Big Data*, vol. 6, no. 1, p. 113, Dec. 2019, doi: 10.1186/s40537-019-0276-2.
- [47] C. Szegedy, V. Vanhoucke, S. Ioffe, J. Shlens, and Z. Wojna, “Rethinking the Inception Architecture for Computer Vision,” *Proceedings of the IEEE Computer Society Conference on Computer Vision and Pattern Recognition*, vol. 2016-Decem. pp. 2818–2826, 2016. doi: 10.1109/CVPR.2016.308.
- [48] S. Ruder, “An overview of gradient descent optimization algorithms,” pp. 1–14, 2016.
- [49] M. Buckland and F. Gey, “The relationship between recall and precision,” *J. Am. Soc. Inf. Sci.*, vol. 45, no. 1, pp. 12–8231, 1994.
- [50] J. Davis and M. Goadrich, “The relationship between Precision-Recall and ROC curves,” 2006, pp. 233–240.
- [51] F. X. Diebold and R. S. Mariano, “Comparing predictive accuracy,” *J. Bus. Econ. Stat.*, vol. 20, no. 1, pp. 15–134, 2002.
- [52] M. Sokolova, N. Japkowicz, and S. Szpakowicz, “Beyond accuracy, F-score and ROC: a family of discriminant measures for performance evaluation,” 2006, pp. 1015–1021.
- [53] C. Cortes and M. Mohri, “Confidence intervals for the area under the ROC Curve,” *Advances in Neural Information Processing Systems*. 2005.
- [54] L. Van Der Maaten and G. Hinton, “Visualizing Data using t-SNE,” *J. Mach. Learn. Res.*, vol. 9, pp. 2579–2605, 2008.